Supporting information for "Elastic amplification of the Rayleigh-Taylor instability in solidifying melts"

Etienne Jambon-Puillet[1], Matthieu Royer Piéchaud[1], P.-T. Brun[1]
[1]*Department of Chemical and Biological Engineering, Princeton University,Princeton, New-Jersey 08540, USA*
(Dated: December 4, 2020)

In this supplementary document, we provide a supplementary figure relevant for the materials and methods, describe the supplementary movies and provide additional experimental results. In addition, we derive the energy of the pulled drop [Eq. (2) of the main text] and discuss the limitations of our model at large strain ($\alpha \gtrsim 8$).

I. METHODS FIGURE, ADDITIONAL EXPERIMENTAL RESULTS AND SUPPLEMENTARY MOVIES DESCRIPTION

Fig. S1 is referenced within the materials and methods section of the main text.

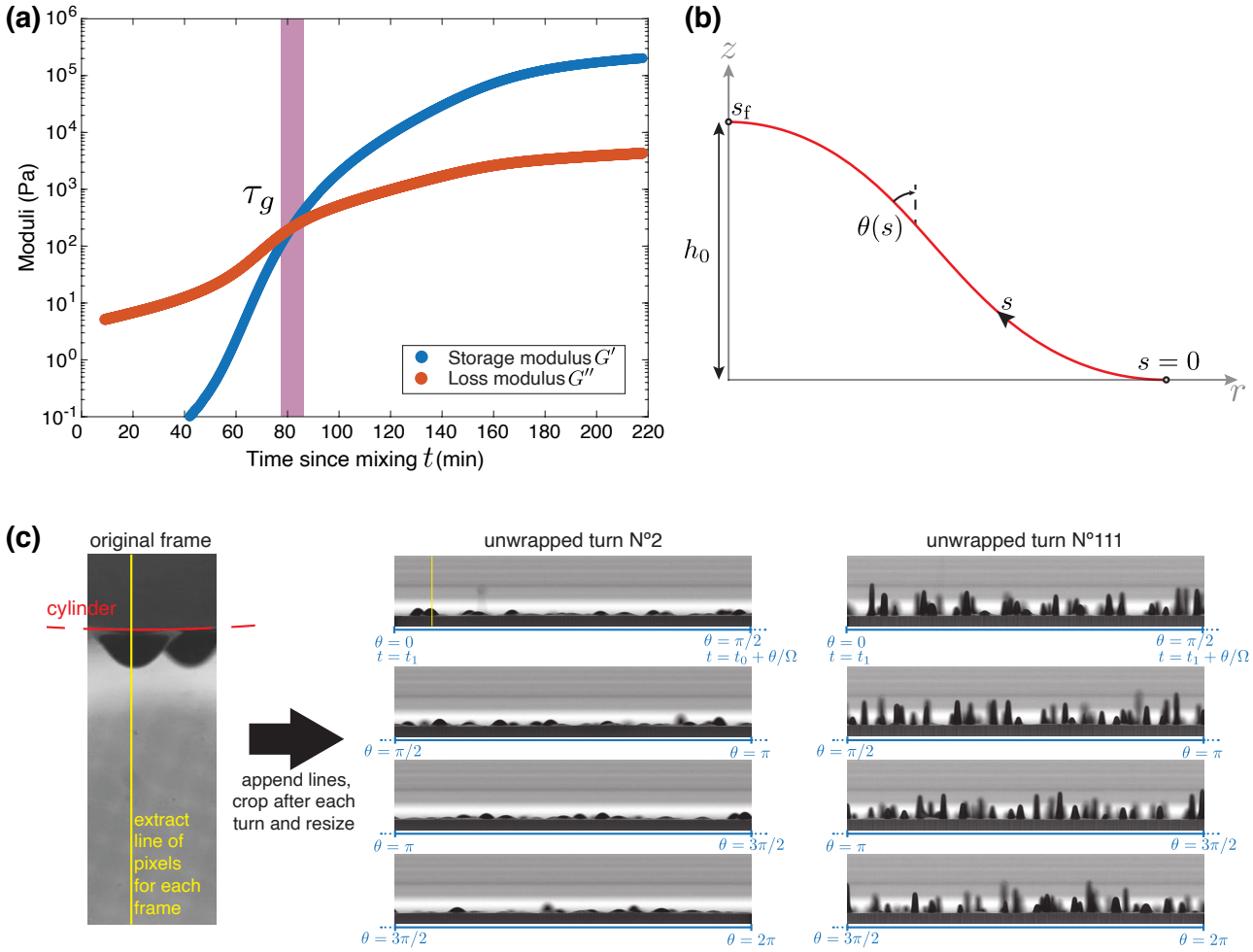

FIG. S1. **(a)** Storage and loss moduli obtained for PDMS with curing accelerator, strain 5%, frequency 0.3 Hz. **(b)** Schematic of a pendant drop defining the coordinates used for the numerical integration. **(c)** Schematic describing the unwrapping of the cylinder. A radial line of pixel is extracted from each frame. These lines are then appended horizontally to form a spatio-temporal diagram which unwraps the drops from the whole cylinder. A mark on the cylinder allows us to detect each full rotation on the spatio-temporal diagram which is then cropped horizontally to have a sub-diagram for each turn. The diagram is then resized horizontally to recover the original drop aspect ratio.

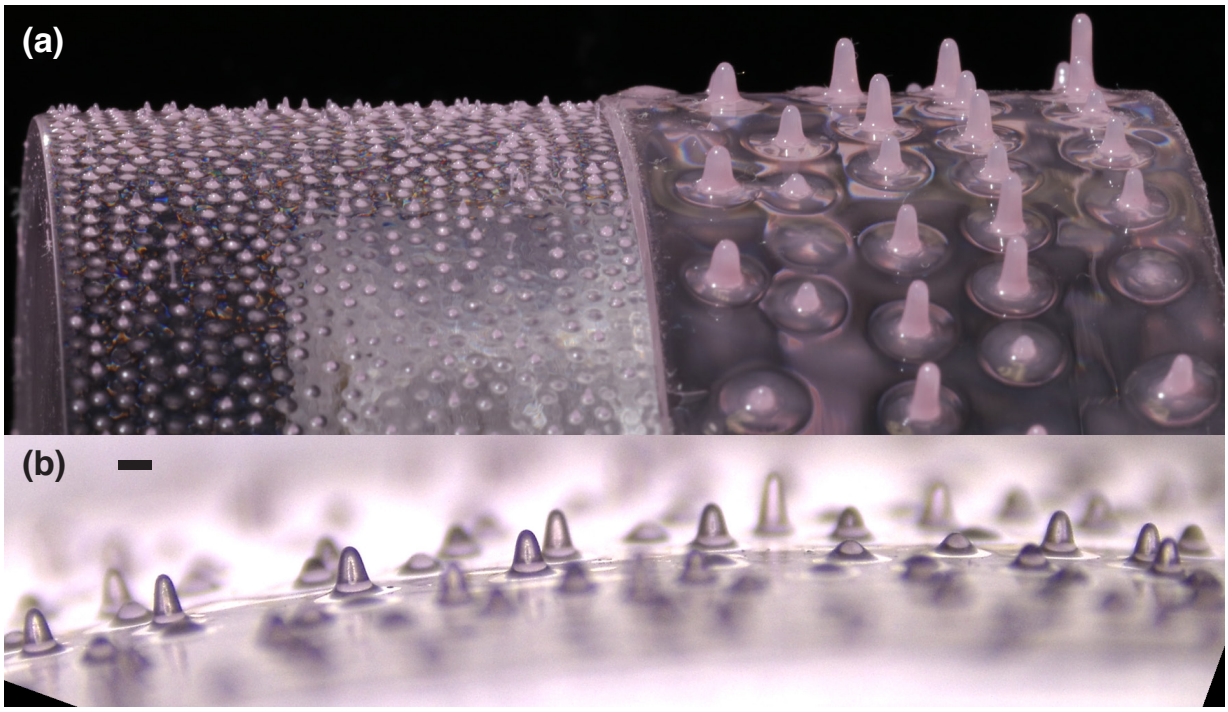

FIG. S2. **(a)** Side by side comparison of VPS-8 hairs of different size obtained by varying the initial rotation speed Ω_1. On the left $\Omega_1 = 1800$ RPM, $\Omega_2 = 5000$ RPM. On the right $\Omega_1 = 400$ RPM, $\Omega_1 = 1000$ RPM. **(b)** Close up view of the left pattern in (a). scale bar 300 μm.

Fig. S2 demonstrate the possibility to scale down the hair pattern by scaling down the seed droplets size as described in our previous work [1]. Hairs similar to the ones in the main text are displayed on the right of Fig. S2 (a). They were obtained with $\Omega_1 = 400$ RPM which results in seed droplets with a typical size $\ell_c \approx 0.5$ mm. By increasing the initial rotation speed to $\Omega_1 = 1800$ RPM, we decreased the seed droplet size to $\ell_c \approx 0.12$ mm which allowed us to make the smaller hairs shown on the left of Fig. S2 (a). A close up view of the smaller hairs is shown in Fig. S2 (b) and confirm that their shape is similar to the larger ones. However, the faster rotation speed induced a faster curing such that we had to adjust the value of t^*.

Movie S1 shows the PDMS multi-step experiment described in Fig. 2 once unwrapped. Close-up views are displayed in the colored boxes.

Movie S2 shows a VPS-8 experiment where a continuous ramp in speed (300 $\rightarrow$ 1800 RPM) was applied to the sample. Here we exceeded the yield point, resulting in large deformations and tearing of the hairs.

Movie S3 illustrate the loss of axisymmetry and void formation observed at the base of the hairs at large strain by rotating on a platform a VPS-8 hair cut from the pattern.

II. MODEL

The deformation of an hyperelastic drop due to the change in centrifugal acceleration is computed by minimizing the total energy of the drop, which is the sum of the elastic (or strain) energy and the gravitational potential energy. Placing ourselves in the drop's frame of reference, the body force (acceleration) is vertical, i.e. along z in the usual Cartesian coordinates. We assume that the deformation is homogeneous such that the principal stretches (λ_x, λ_y, λ_z) are isotropic and that the hairs remain axisymmetric such that $\lambda_x = \lambda_y$. Incompressibility finally imposes $\lambda_x\lambda_y = 1/\lambda_z$ and denoting $\lambda_z = \lambda = h/h_0$, the principal stretches are therefore ($\lambda^{-1/2}$, $\lambda^{-1/2}$, λ). Consequently, the initial and deformed drop shapes are self-similar as shown in Fig. S3(a). We compare the assumed homogeneous deformation to experiments in Fig. S3(b). Although the agreement is not perfect, as it could be expect from such a simplistic assumption, the hair shape is still reasonably captured. Because the stretch are isotropic, the total strain energy is $\mathcal{E}_{\text{ela}} = \iiint_{V_0} \mathcal{W}\, \mathrm{d}^3\mathbf{r} = \mathcal{W}V_0$ with $\mathcal{W}$ the strain energy density and V_0 the drop initial volume. For a Neo-Hookean drop of shear modulus G we get:

$$\mathcal{E}_{\text{ela}} = \frac{GV_0}{2}\left(\lambda^2 + \frac{2}{\lambda} - 3\right). \tag{S1}$$

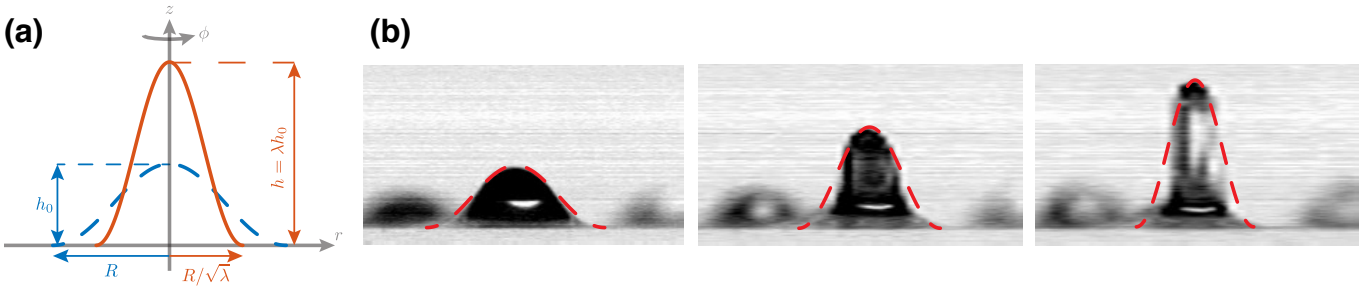

FIG. S3. **(a)** Schematic showing the initial drop shape (dashed curve) in cylindrical coordinate (r,ϕ,z) and its deformed shape (dashed curve) after applying the homogeneous deformation $(\lambda^{-1/2},\lambda^{-1/2},\lambda)$. **(b)** Comparison between experimental drop and hair shapes [from Fig. 2(b)] and the simplified homogeneous deformation assumed in our model. The leftmost curve is the small-slope drop shape, i.e. equation (S3).

The drop gravitational energy is $\mathcal{E}_g = \iiint_V \rho g_{\text{eff}} z \, \mathrm{d}^3\mathbf{r}$ with g_{eff} the centrifugal acceleration (assumed constant over the drop since $R \gg h$) and V the volume of the deformed drop. Introducing the cylindrical coordinate centered at the drop base [see Fig. S3(a)] and defining the deformed drop surface with $\{r,z\}$ we have $\mathcal{E}_g = \pi\rho g_{\text{eff}} \int_0^h z r^2(z)\,\mathrm{d}z$ from axisymmetry. We can reduce the integral over the deformed shape to an integral over the undeformed shape $\{r_0,z_0\}$ using the change of variables $(z_0 = z/\lambda,\, r_0 = \sqrt{\lambda} r)$ which yields $\mathcal{E}_g = \pi\lambda\rho g_{\text{eff}} \int_0^{h_0} z_0 r_0^2(z_0)\,\mathrm{d}z_0$. Using the theoretical drop shapes we obtained by numerically solving the Young-Laplace equation [Eq. (5)] we get

$$\mathcal{E}_g = \beta \rho g_{\text{eff}} h_0 V_0 \lambda \tag{S2}$$

after numerically evaluating the integral with β a number that varies between $0.289 < \beta < 0.300$ depending on the exact profile used. This result can be derived analytically by considering the small slope solution of pendant drops [2]

$$\frac{z_0(r_0)}{h_0} = \frac{\mathrm{J}_0(R/\ell_c) - \mathrm{J}_0(r_0/\ell_c)}{\mathrm{J}_0(R/\ell_c) - 1}. \tag{S3}$$

Here, J_0 is the Bessel function of the first kind of order 0 and $R \approx 3.83\ell_c$ is the drop radius defined by $\mathrm{J}_0'(R/\ell_c) = 0$. As shown on the leftmost picture of Fig. S3(b), Eq. (S3) is a good analytical approximation of the drop shapes. Using it to compute the gravitational energy we recover Eq. (S2) with $\beta = \mathrm{J}_0(R/\ell_c)/\left(\mathrm{J}_0(R/\ell_c) - 1\right) \approx 0.287$, very close to our previous numerical estimation.

The total energy of the drop is finally $\mathcal{E} = \mathcal{E}_{\text{ela}} - \mathcal{E}_g$ or

$$\mathcal{E} = \frac{GV_0}{2}\left(\lambda^2 + \frac{2}{\lambda} - 3\right) - \beta\rho g_{\text{eff}} h_0 V_0 \lambda, \tag{S4}$$

which is equivalent to Eq. (2) of the main text. Minimizing the energy finally yields

$$\frac{\partial \mathcal{E}}{\partial \lambda} = GV_0\left(\lambda - \frac{1}{\lambda^2} - \beta\alpha\right) = 0,$$

which becomes the cubic equation in the main text after multiplying both sides by $\lambda^2/(GV_0)$.

III. LIMITATIONS OF OUR ELASTIC FRAMEWORK

When the dimensionless acceleration exceeds $\alpha \gtrsim 8$, or equivalently when the drop stretch exceeds $\lambda \gtrsim 250\%$, our Neo-Hookean elastic framework no longer reproduces the deformations observed quantitatively. In Fig. S4(a) we plot the stretch $\lambda = h/h_0$ as a function of the dimensionless gravity $\alpha = \rho g_{\text{eff}} h_0/G$ for individual drop as in Fig. 3 of the main text, but this time including data for very large deformations obtained with a very soft PDMS melt. As shown the stretch at high accelerations is higher than predicted by both the FEM (with G calibrated at small deformations) and the model. Representative images of the experiment are shown in Fig. S4(b) and a high resolution image of a similar experiment done with VPS-8 is shown in Fig. S4(c). At these high deformations the drops loose axisymmetry and develop one or multiple voids at their base illustrated in Fig. S4(c) and movie S3. These voids are reminiscent of the elastic fingering and fringe instabilities that occurs in stretched hyperelastic solids [3–5]. However, theses instabilities are quantitatively reproduced by 3D FEM simulations [4] which is not the case of

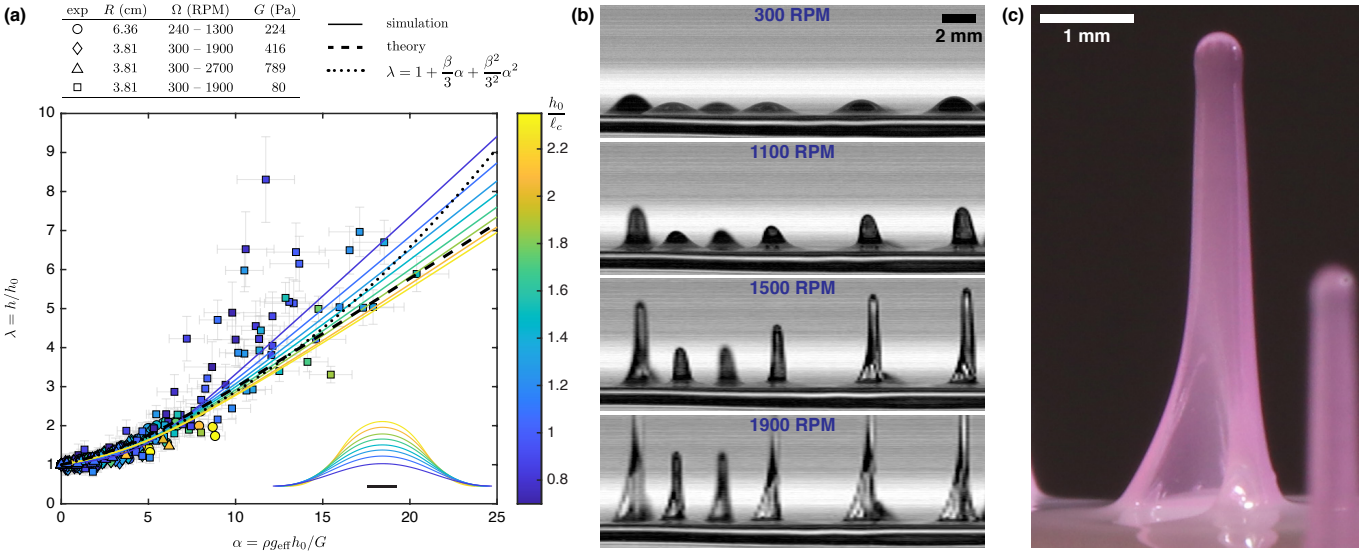

FIG. S4. **(a)** Stretch $\lambda = h/h_0$ as a function of the dimensionless gravity $\alpha = \rho g_{\rm eff} h_0/G$, including data for very large deformations. The legend is identical to Fig. 3 of the main text. **(b)** Snapshots of a representative portion of the fast camera reconstructed images of the experiment shown as squares in (a). The values of the dimensionless gravity for the rightmost drop are from top to bottom $\alpha = \{0 - 6.7 - 12.9 - 20.9\}$. **(c)** High-resolution image of a cured VPS-8 drop exhibiting similar deformations, with the formation of a void at the base of the drop.

the voids we observe in our experiments. This suggests that other physical effects come into play and shows the limitations of our Neo-Hookean purely elastic framework. Because the voids appear at high stretch and at the base of the hairs where the elastic energy is highest, we hypothesize that they result from viscous or plastic effects. Eventually at even higher accelerations $\alpha \gtrsim 20$ (or $\lambda \gtrsim 1000\%$), the hairs get teared off (see Movie S2). These thresholds roughly coincide for PDMS and VPS-8 but are probably material dependent. The teared morphology is for instance different between PDMS and VPS-8, the former displaying viscous like filaments while the latter appears more brittle with very little material left on the cylinder.

[1] J. Marthelot, E. F. Strong, P. M. Reis, and P.-T. Brun, Nature Communications **9**, 4477 (2018).
[2] J. R. Lister, J. M. Rallison, and S. J. Rees, Journal of Fluid Mechanics **647**, 239–264 (2010).
[3] K. R. Shull, C. M. Flanigan, and A. J. Crosby, Phys. Rev. Lett. **84**, 3057 (2000).
[4] S. Lin, T. Cohen, T. Zhang, H. Yuk, R. Abeyaratne, and X. Zhao, Soft Matter **12**, 8899 (2016).
[5] S. Mora, E. Andò, J.-M. Fromental, T. Phou, and Y. Pomeau, Soft Matter **15**, 5464 (2019).